

# Thermal Motors with Enhanced Performance due to Engineered Exceptional Points

Lucas J. Fernández-Alcázar, Rodion Kononchuk, Tsampikos Kottos  
*Wave Transport in Complex Systems Lab, Department of Physics,  
 Wesleyan University, Middletown, CT-06459, USA*  
 (Dated: October 19, 2021)

A thermal current, generated by a temperature gradient between two reservoirs coupled to a carefully designed photonic or (micro-) electromechanical circuit, might induce non-conservative forces that impulse a mechanical degree of freedom to move along a *closed trajectory*. We show that in the limit of long - but finite - modulation periods, the extracted power and the efficiency of such autonomous motors can be maximized when an appropriately designed spatio-temporal symmetry violation is induced and when the motor operates in the vicinity of exceptional point (EP) degeneracies. These singularities appear in the spectrum of the effective non-Hermitian Hamiltonian that describes the combined circuit-reservoirs system when we judiciously tailor the coupling between them. In the photonic framework, these motors can be propelled by thermal radiation and can be utilized as autonomous self-powered microrobots, or as micro-pumps for microfluidics in biological environments. The same designs can be also implemented with electromechanical elements for harvesting ambient mechanical (or electrical) noise for powering a variety of auxiliary systems.

## I. INTRODUCTION

The manipulation of microscopic objects via currents has become an indispensable tool in many disciplines of science and technology, revolutionizing a variety of applications in areas as diverse as micro-engineering and micro-robotics, to biology and medicine<sup>1–10</sup>. Depending on the application, the source of these currents varies from thermal radiation and thermal vibrations to electrical and chemical energy extracted in biological processes. On the fundamental level, such applications require the development of design principles that will allow us to realize powerful and efficient engines that operate between two reservoirs at different “temperatures” (or chemical potentials), and produce useful work with maximum efficiency. In particular, in the framework of thermal engines, the question of maximum efficiency has been addressed by the pioneering work of Carnot which pointed out that the efficiency of a thermal engine that performs a cycle between two reservoirs with temperatures  $T_H$  and  $T_C$  ( $T_H > T_C$ ) is bounded by the so-called Carnot efficiency  $\eta_C = 1 - T_C/T_H$ <sup>11,12</sup>. Of course, this thermodynamic bound is of limited practical importance since the corresponding heat engine must work reversibly, and thus its output power is zero. A more practical direction is to identify conditions under which the power of *irreversible* thermal engines, working under finite-time Carnot cycles, is optimized while their efficiency is still high<sup>13–18</sup>. The situation is even more complex when one abandons the convenience of macroscopic thermodynamics framework and delves into the challenges of modern nano-devices, where wave interferences and thermal fluctuations dominate their performance<sup>19–22</sup>.

A prominent framework where many of these challenges met is in photonics. In this case, the near field thermal radiation, emitted from a hot reservoir towards a cold reservoir, can be harvested by an optomechanical circuit as a non-conservative “wind-force”. Under its influence, a (slow) mechanical degree of freedom (MDF)

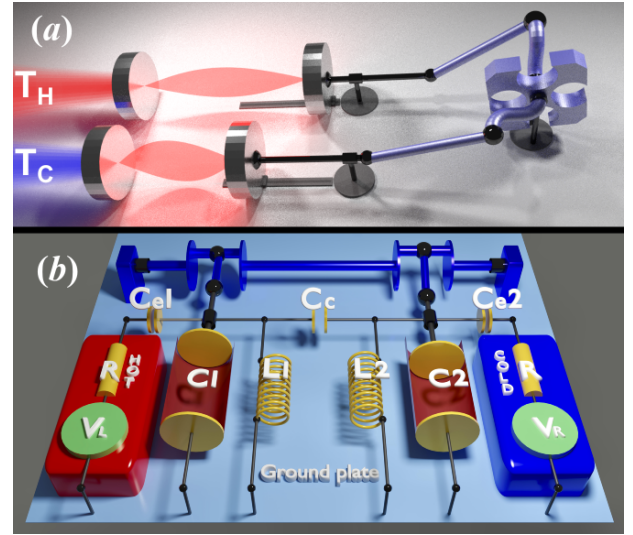


FIG. 1. Schematic representation of our thermal motor. (a) A photonic circuit connected to two thermal baths at different temperatures  $T_H > T_C$  is able to divert part of the thermal radiative energy into useful work in the form of the motion of a mechanical degree of freedom (MDF) described by a rotor. (b) An electromechanical motor consisting of two coupled LC resonators. The capacitance plates of the LC circuits are coupled to pistons whose motion is out-of-phase with one another, thus exceeding a torque to a rotor. When the system operates in the vicinity of EPs and violates specific spatio-temporal symmetries, (or the baths are subjected to spectral filtering), the motor operates at optimal performance.

undergoes a closed path periodic motion. We show that for a long - but finite - driving period of the MDF, these circuits act as *autonomous radiative motors*, whose extracted power and efficiency are maximized when they are designed to operate in a domain of their parameter space which is in the vicinity of an exceptional point (EP) degeneracy. The latter signifies a coalescence of the eigenvalues and the corresponding eigenvectors of the ef-

fective non-Hermitian Hamiltonian that describes the coupling of these motors with the thermal reservoirs. We have engineered such EPs via a judicious coupling contrast with the reservoirs and we have harvested its influence in the enhancement of the performance of the motor, by appropriate manipulation of its spatio-temporal symmetries and of the thermal emissivity of the attached reservoirs. Our predictions can guide the design towards optimal operational conditions of autonomous motors. Their applicability extends beyond the photonic framework to other platforms like electromechanical circuits for harvesting mechanical (e.g. vibrational) ambient noise for power supply of a variety of auxiliary systems<sup>23–28</sup>.

## II. MATHEMATICAL FORMULATION

The system consists of two thermal reservoirs at different temperatures  $T_H > T_C$ , which are brought in contact via a circuit. The latter is coupled to a MDF from which we extract work. For simplicity, we will assume that the circuit incorporates two single-mode resonators whose frequencies  $\omega_n$  (where  $n = 1, 2$ ) are modulated by the motion of the MDF. The temperature gradient between the two reservoirs produces a thermal current through the circuit that, in turn, exerts a force to the MDF engaging them in slow periodic motion along a given closed trajectory  $\mathcal{C}$  in a parameter space. The design is chosen in a way that the motion along the path  $\mathcal{C}$  creates out-of-phase variations in  $\omega_{1,2}$ , thus leading to a violation of spatio-temporal symmetries of the structure. One possible implementation of the above set-up is in the photonic framework Fig. 1a, while a parallel proposal in the electromechanical framework is shown in Fig. 1b. Below, we will mainly use the photonic “language” associated with Fig. 1a, while we will also have the electromechanical scenario of Fig. 1b in mind.

In typical circumstances, the MDF  $\vec{X} = \{X_1, X_2, \dots, X_M\}$  describes a change in position or angle of the mechanical element due to a respective force or torque. For concreteness of our presentation, we will assume that  $M = 2$ . The coordinate  $\vec{X}$  abides by the Langevin equation

$$\mathcal{M}\ddot{\vec{X}}(t) = \Gamma\dot{\vec{X}}(t) + \vec{F}_{\text{av}} + \vec{\xi}(t), \quad (1)$$

where  $\mathcal{M}$  is the generalized inertia tensor,  $\vec{\xi}(t)$  is a fluctuating force and  $\Gamma$  is the friction tensor which satisfies a fluctuation-dissipation relation. In our analysis below, we will assume that the fluctuating force  $\vec{\xi}$  can be neglected due to the large inertia of the MDF. Consequently, we can approximate the dynamics of  $\vec{X}$  by its mean value  $\vec{x} = \langle \vec{X} \rangle$ , where  $\langle \cdot \rangle$  indicates a thermal averaging. Finally, the mean “force”  $\vec{F}_{\text{av}}$ , drives the mechanical rotor diverting energy from the “photonic” thermal current to produce mechanical work. In the photonic framework (Fig. 1a)  $\vec{F}_{\text{av}}$  is analogous to the radiation pressure asso-

ciated with the radiation inside the circuit. In the electromechanical framework of Fig. 1b,  $\vec{F}_{\text{av}}$  is associated with a torque acting on the mechanical rotor.

The interaction between the mechanical part and the radiation is obtained from the variation of the energy inside the photonic circuit due to a displacement  $\vec{x}$  of the MDF. Specifically, the thermal averaged force is

$$\vec{F}_{\text{av}} = -\hbar \left\langle \Psi^\dagger \frac{\partial H_0}{\partial \vec{x}} \Psi \right\rangle = -\hbar \sum_{n,n'} \left( \frac{\partial H_0}{\partial \vec{x}} \right)_{nn'} \langle \psi_n(t)^* \psi_{n'}(t) \rangle. \quad (2)$$

where  $\Psi = (\psi_1, \dots, \psi_N)^T$ ,  $\psi_n$  is the field amplitude at the  $n$ -th resonator of the circuit ( $\hbar\omega_n |\psi_n|^2$  represents the energy density in the  $n$ -th mode/resonator), and  $H_0(\vec{x})$  is the effective Hamiltonian of the circuit that provides a description of the dynamics of the radiation field in the single-mode resonators. The dynamics of the open system (circuit coupled with reservoirs) is described in terms of a temporal coupled-mode theory (CMT)<sup>29</sup>

$$i \frac{d\Psi(t)}{dt} = H_{\text{eff}} \Psi(t) + iD^T \theta^{(+)}(t); \quad H_{\text{eff}} = H_0(\vec{x}) - i \frac{D^T D}{2} \\ \theta^{(-)} = -\theta^{(+)} + D\Psi; \quad (3)$$

where the matrix  $D$ , with elements  $D_{n,\alpha} = \sqrt{2\gamma_\alpha} \delta_{n,\alpha}$ , describes the coupling of the circuit with the thermal baths. The thermal excitations from (towards) the  $\alpha$ -th reservoir are given by the incoming (outgoing) complex fields  $\theta^{(+)} [\theta^{(-)}]$ . In the frequency domain (using the Fourier transform  $f(t) = \int_0^\infty f(\omega) e^{-i\omega t} d\omega$ ), the amplitudes  $\theta_\alpha^{(+)}(\omega)$  satisfy the relation

$$\left\langle [\theta_{\alpha'}^{(+)}(\omega')]^* \theta_\alpha^{(+)}(\omega) \right\rangle = \frac{1}{2\pi} \tilde{\Theta}_\alpha(\omega) \delta(\omega - \omega') \delta_{\alpha,\alpha'} \quad (4)$$

where  $\tilde{\Theta}(\omega) = \Phi(\omega) \cdot \Theta(\omega)$ , with  $\Phi(\omega)$  being a noise filter function and  $\Theta_\alpha(\omega) = \{\exp[\hbar\omega/(k_B T_\alpha)] - 1\}^{-1}$  is the Bose-Einstein statistics describing the mean number of photons which are emitted from reservoir  $\alpha$  with frequency  $\omega$ . Finally  $T_\alpha$  is the temperature of the  $\alpha$ -th reservoir.

## III. WORK

We assume that the dynamics of the MDF Eq. (1) occurs on time-scales much larger than the ones associated with the field dynamics Eq. (3). Under this assumption, we can invoke the Born-Oppenheimer approximation and obtain the work performed by the motor along the path  $\mathcal{C}$  as<sup>30–36</sup> (see supplement)

$$W = \int_0^\infty \frac{d\omega}{2\pi} \sum_\alpha \tilde{\Theta}_\alpha(\omega) P_\alpha(\omega); \quad (5) \\ P_\alpha = \frac{\hbar}{i} \oint_{\mathcal{C}} d\vec{x} [(S^{\vec{x}})^\dagger \nabla_{\vec{x}} S^{\vec{x}}]_{\alpha,\alpha} = \hbar \oint_{\mathcal{C}} R^{\vec{x}} \nabla_{\vec{x}} \alpha^{\vec{x}} d\vec{x}.$$

where  $S^{\vec{x}}(\omega) = -I_{N_\alpha} + iDG^{\vec{x}}(\omega)D^T$  is the unitary instantaneous scattering matrix, and  $G^{\vec{x}} = [\omega I_N - H_{\text{eff}}(\vec{x})]^{-1}$  is

the Green's function associated with the effective Hamiltonian  $H_{\text{eff}}$  ( $I_m$  is the  $m \times m$  identity matrix). In Eq. (5), the kernel  $P_\alpha(\omega)$  indicates the spectral response of the system at a frequency  $\omega$ . Since  $P_\alpha(\omega)$  only involves a parametric integral along the path  $C$ , it is a geometric quantity<sup>37,38</sup>. It turns out that for the two-reservoir setup of Fig. 1,  $P_\alpha$  can be written only in terms of the reflectance  $R^{\vec{x}}$  and the corresponding reflection phase  $\alpha^{\vec{x}}$  (see the right part of Eq. (5)). As a matter of convention, a positive  $W$  in Eq. (5) indicates that the dynamics of  $\vec{x}$  follows the positive direction of the path  $C$ .

An analytically useful expression of  $P_\alpha$  is achieved by substituting in Eq. (5) the scattering matrix in terms of the Green's function. We get

$$P_\alpha = \iint_A \frac{\partial \omega_p}{\partial x_p} \frac{\partial \omega_q}{\partial x_q} \mathcal{W}_\alpha dx_p dx_q, \quad (6)$$

where we have used that  $\left(\frac{\partial H_0}{\partial x_p}\right)_{n,m} = \frac{\partial \omega_n}{\partial x_p} \delta_{n,m} \delta_{n,p}$ , and we have introduced the work density per unit area as

$$\mathcal{W}_\alpha = \lim_{A \rightarrow 0} P_\alpha/A = 4\gamma_\alpha \hbar \text{Re} (G_{p\alpha}^* G_{pq} G_{q\alpha} - G_{q\alpha}^* G_{qp} G_{p\alpha}), \quad (7)$$

with  $A = \iint_A \frac{\partial \omega_p}{\partial x_p} \frac{\partial \omega_q}{\partial x_q} dx_p dx_q \rightarrow 0$ .

Direct inspection of Eq. (5) allow us to establish the following two conditions for the implementation of our proposal as a motor: (a) the force has to be non-conservative which means that the  $\nabla_{\vec{x}} \times [(S^{\vec{x}})^\dagger \nabla_{\vec{x}} S^{\vec{x}}]_{\alpha,\alpha} \neq 0$ , and (b) the closed path  $C$  must enclose a non-zero area in the parameter space  $\{x_1, x_2\}$ . A bi-product of the last condition is that variations of  $x_1, x_2$  with a phase difference 0 or  $\pi$  cannot produce work.

#### IV. ENGINEERING EP DEGENERACIES

In the frequency range near an EP-degeneracy the resolvent of the effective Hamiltonian  $H_{\text{eff}}$  can be approximated by a  $2 \times 2$  subspace involving only the resonant modes associated with the EP. We therefore consider a minimal model consisting of two coupled modes with resonant frequencies  $\omega_1, \omega_2$ . Alternatively, one can consider, as a concrete example, the set-up of Fig. 1a. The system consists of two single-mode resonators coupled asymmetrically to two reservoirs at temperatures  $T_{\alpha=1} = T_H$  and  $T_{\alpha=2} = T_C$ . The effective Hamiltonian of such a reduced system reads

$$H_{\text{eff}} = \begin{pmatrix} \omega_1 - i\gamma_1 & \kappa \\ \kappa & \omega_2 - i\gamma_2 \end{pmatrix} \quad (8)$$

where  $\kappa$  describes the coupling between the two modes and  $\gamma_1, \gamma_2$  are the (asymmetric) decay rates of the two modes due to their coupling with the two reservoirs. The spectrum of  $H_{\text{eff}}$  is  $\omega_\pm = \omega_0 - i\gamma_0 \pm \frac{1}{2}\sqrt{(\Delta\omega - i\Delta\gamma)^2 + 4\kappa^2}$ , where  $\omega_0 = \frac{\omega_1 + \omega_2}{2}$ ,  $\gamma_0 = \frac{\gamma_1 + \gamma_2}{2}$  and  $\Delta\omega = \omega_1 - \omega_2$  and  $\Delta\gamma = \gamma_1 - \gamma_2 \neq 0$ . The

corresponding (non-normalized) eigenvectors are  $u_{1,2} = \left(2\kappa, -\Delta\omega + i\Delta\gamma \pm \sqrt{(\Delta\omega - i\Delta\gamma)^2 + 4\kappa^2}\right)$ . It is easy to show that when  $\Delta\omega = \Delta\omega_{\text{EP}} = 0$  and  $\kappa_{\text{EP}} = \Delta\gamma/2$  the system supports an EP degeneracy with  $\omega_+ = \omega_- = \omega_{\text{EP}} = \omega_0 - i\gamma_0$ .

In fact, under the condition  $\Delta\omega = \Delta\omega_{\text{EP}}$ , the Hamiltonian Eq. (8) respects a (pseudo-)parity-time ( $\mathcal{PT}$ ) symmetry that reveals itself after renormalizing the losses with respect to their mean value  $\gamma_0$ <sup>39</sup>. Below we will be discussing in detail two distinct scenarios involving perturbations around the EP that violate this (pseudo-)  $\mathcal{PT}$ -symmetry either spontaneously or explicitly. We will show that each of these cases affects in a dramatically different manner the characteristic features of the work density  $\mathcal{W}_\alpha$ .

#### V. WORK DENSITY IN THE PRESENCE OF AN EP

We analyze the extracted work density of the motor when the center of the modulation cycle is in the proximity of an EP. To this end, we consider a modulation cycle  $C$  associated with changes of the resonant frequencies being  $\omega_n = \omega_0 (1 + \delta \cos(x_n + \phi_n)) - (-1)^n \epsilon$ , where  $\epsilon$  describes a resonance detuning that displace the unmodulated system Eq. (8) from the EP by violating explicitly its (pseudo-)  $\mathcal{PT}$ -symmetry. In order to satisfy the criteria for non-zero work, we have assumed that the two resonances are modulated out of phase i.e.  $\phi_1 = \pi/2, \phi_2 = 0$ . For such a modulation scenario, the associated enclosed area in the parameter space  $(\omega_1(x_1), \omega_2(x_2)) / \omega_0$  is  $A = \pi\delta^2$ .

Next, we assume a generic perturbation  $p$  which displaces the center of the modulation cycle with respect to the EP. Using Eq. (7), we have evaluated the work density  $\mathcal{W}_\alpha$  in terms of the Green's function  $G^{\vec{x}}$ . In fact, for the  $2 \times 2$  case, the calculations for the Green's function can be carried out explicitly for any perturbation, giving

$$G^{\vec{x}} = \frac{1}{D} \begin{pmatrix} \omega - (\omega_2 - i\gamma_2) & -\kappa \\ -\kappa & \omega - (\omega_1 - i\gamma_1) \end{pmatrix} \approx \frac{A}{\omega - \omega_{\text{EP}}} + \frac{B}{(\omega - \omega_{\text{EP}})^2}, \quad (9)$$

where  $D = [\omega - (\omega_2 - i\gamma_2)][\omega - (\omega_1 - i\gamma_1)] - \kappa^2$ . In the above expression, the generic perturbation  $p$  is "hidden" in the parameters that define  $H_{\text{eff}}$  e.g. in the frequencies  $\omega_{1,2} = \omega_{1,2}(p)$  and/or the coupling  $\kappa = \kappa(p)$  between the two resonant modes. When  $p \rightarrow 0$  the Green's function can be approximated with the last expression, where  $A$  and  $B$  are frequency-independent matrices (see methods). It turns out that the functional dependence of  $\mathcal{W}_\alpha$  on  $\omega$ , in the vicinity of the EP, is dramatically affected by the presence of the square-Lorentzian term on the last part of Eq. (9). This unique spectral feature is a consequence of the degeneracy of the eigenvectors of  $H_{\text{eff}}$  at the

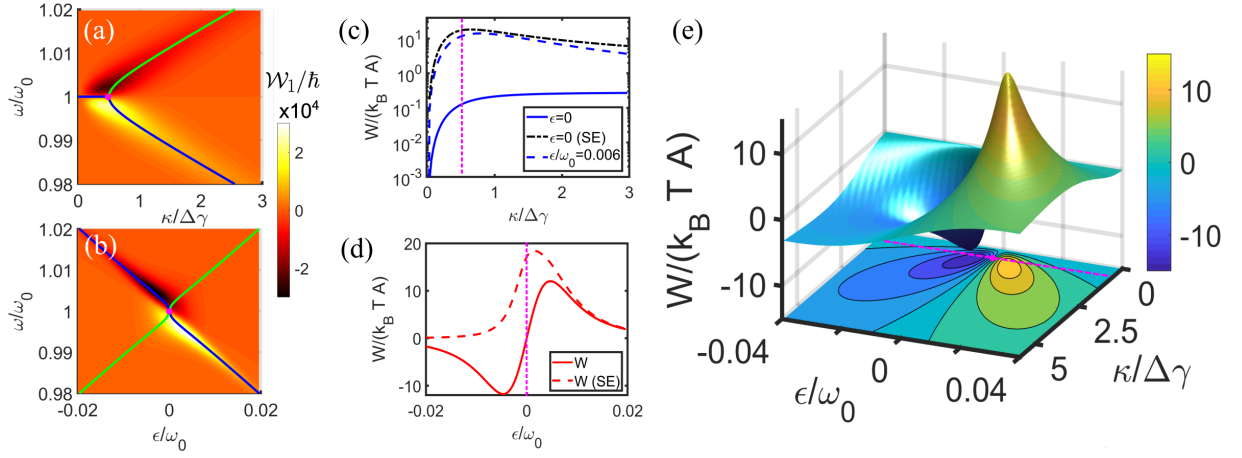


FIG. 2. **Work in the proximity of an EP.** (a) and (b) The work density (color scale) as a function of the coupling constant  $\kappa$  and frequency  $\omega$  of the incident radiation. Blue and green solid lines are the eigenfrequencies of  $H_{\text{eff}}$  which they demonstrate an EP degeneracy (indicated by the magenta point) at  $\kappa/\Delta\gamma = 0.5$  in (a) and at  $\epsilon = 0$  in (b). (a) In the absence of a resonance detuning, i.e.,  $\epsilon = 0$ , the work density is maximized (minimized) close to the EP for frequencies  $\omega < \text{Re}(\omega_{\text{EP}})$  [ $\omega > \text{Re}(\omega_{\text{EP}})$ ]. (b) A nonzero detuning, i.e.,  $\epsilon \approx 0.006\omega_0$ , breaks the symmetry along the frequency axis. Here  $\kappa/\Delta\gamma = 0.5$ . (c) The work  $W$  for  $\epsilon = 0$  ( $\epsilon = 0.006\omega_0$ ) is indicated with a solid (dashed) blue line respectively. At the same subfigure, we report (short dashed black line) the work in the case where we have introduced a spectral filtering function  $\Phi(\omega) = H(\omega - \omega_0)$  ( $H(x)$  is the Heaviside function). (d) Work with spectrally engineered reservoirs for  $\epsilon = 0$  (solid red line) and  $\epsilon \approx 0.006\omega_0$  (dashed red line). From subfigures (c) and (d) we conclude that a perturbation that explicitly violates the (pseudo)- $\mathcal{PT}$ -symmetry (e.g. due to resonant detuning) or/and appropriate spectral filtering of the bath maximizes the work  $W$  in the parameter-space domain which is in the proximity to the EP. In the above examples, the resulting enhancement factor is  $\sim 200$ -fold as opposed to the unperturbed/unfiltered case. **Total work** (e) We report the work  $W$  as a function of the coupling constant  $\kappa$  and the perturbation  $\epsilon$ . The EP parameters are indicated with a magenta dot in the colormap (the magenta line indicates the value of  $\kappa_{\text{EP}}$ ). In the vicinity of the EP, the work becomes extreme (positive or negative). The CMT parameters used in these calculations are:  $\omega_0 = 200 \times 10^{12} \text{rad/s}$ ,  $T_1 = 10^9 \text{K}$ ,  $T_2 = 3 \text{K}$ , and the rest of parameters are in units of  $\omega_0$ :  $\gamma_1 = 0.01$ ,  $\gamma_2 = 0.002$ ,  $\bar{\omega}_1 = \bar{\omega}_2 = 1$ .

EP. Furthermore, a squared Lorentzian lineshape implies a narrower emission/absorption peak and greater resonant enhancement in comparison with a non-degenerate resonance at the same complex frequency. We will show that the competition between the two terms appearing at the right equality of Eq. (9) determines the conditions under which  $\mathcal{W}_\alpha$  acquires its maximum value (see below).

A more elaborated treatment can extend the above analysis of  $G^{\vec{x}}$ , in order to include any number of modes, by using a degenerate perturbation theory that takes into consideration the singular nature of EPs. In this case, the standard modal decomposition of the Green's function is not applicable since the bi-orthogonal eigenvectors of  $H_{\text{eff}}$  do not span the Hilbert space. Instead, one has to complete the eigenvectors of  $H_{\text{eff}}$  into a basis by introducing the associated Jordan vectors<sup>40</sup>. Following this approach, we can recover the last expression of  $G^{\vec{x}}$  in Eq. (9).

Substituting the expression for the Green's function back in Eqs. (6,7) we get that:

$$\begin{aligned} \mathcal{W}_1 &= 4\hbar\gamma_1\gamma_2\text{Re}\left[\frac{-2i\kappa^2 D^*}{|D|^4}\right] \\ &= \frac{-8\hbar\gamma_1\gamma_2\kappa^2(2\gamma_0(\omega - \omega_0) + \epsilon\Delta\gamma)}{\left\{[(\omega - \omega_0)^2 - \gamma_0^2 - \epsilon^2 + c]^2 + [2\gamma_0(\omega - \omega_0) + \epsilon\Delta\gamma]^2\right\}^2} \mathcal{W}_1(\omega = \omega_0) = 0 = \mathcal{W}_1(\omega \rightarrow \pm\infty) \end{aligned} \quad (10)(11)$$

where for the evaluation of the contour integral in Eq. (6) we have explicitly written  $\omega_{1,2}$  in terms of the parameters  $\omega_0$  and  $\epsilon$  that define the position of the path  $\mathcal{C}$ . The constant  $c = (\Delta\gamma/2)^2 - \kappa^2$  and/or with the detuning  $\epsilon$  indicate the degree of deviation from the EP.

Let us exploit further Eq. (10) by considering two specific examples corresponding to perturbations that preserve/violate the pseudo- $\mathcal{PT}$  symmetry of the effective unmodulated Hamiltonian  $H_{\text{eff}}$ . In the first case, we displace the system away from the EP by varying the coupling  $\kappa \neq \kappa_{\text{EP}}$  while keeping  $\epsilon = 0$ . We find that the work density takes the form

$$\mathcal{W}_1 = -\frac{16\hbar\gamma_1\gamma_2\kappa^2\gamma_0(\omega - \omega_0)}{\left\{[(\omega - \omega_0)^2 + \gamma_0^2 + c]^2 - 4\gamma_0^2 c\right\}^2}. \quad (11)$$

In fact, by considering the EP condition  $c = 0$  we are able to identify in the denominator of  $\mathcal{W}_1$  above, the signature of the square-Lorentzian anomaly associated with the collapse of the eigenvector basis. Equation (10)(11) allows us to conclude that  $\mathcal{W}_1$  is non-monotonic and antisymmetric with respect to the EP resonance frequency axis  $\omega = \omega_0$  for all  $\kappa$ -values. Furthermore, occur in the vicinity of the EP (see the filled magenta

circle) at  $\omega = \omega_0 \pm \sqrt{\frac{1}{7}}\gamma_0$ , see Fig. 2a.

The situation is dramatically different when we choose to perturb the system away from the EP using a parameter that enforces an explicit (pseudo)- $\mathcal{PT}$ -symmetry violation of the unmodulated Hamiltonian  $H_{\text{eff}}$ . An example case is when the resonances of the two coupled modes are detuned by  $\epsilon$ . In this case, the diagonal elements of  $H_{\text{eff}}$  take the form  $\omega_{1,2} = \bar{\omega}_{1,2} \pm \epsilon + \omega_0 \delta \cos(x + \phi_{1,2})$ . Furthermore, the work density does not have a definite symmetry with respect to  $(\omega - \omega_0)$ . To be concrete, we consider the particular case  $\kappa = \kappa_{EP} = \Delta\gamma/2$  for which the work density is

$$\mathcal{W}_1 = -\frac{8\hbar\gamma_1\gamma_2}{|D|^4} \left(\frac{\Delta\gamma}{2}\right)^2 [2\gamma_0(\omega - \omega_0) + \epsilon\Delta\gamma] \quad (12)$$

where now the denominator takes the form  $|D|^4 = \left\{ [(\omega - \omega_0)^2 - \gamma_0^2 - \epsilon^2]^2 + [2\gamma_0(\omega - \omega_0) + \epsilon\Delta\gamma]^2 \right\}^2$  demonstrating the traces of the square-Lorentzian anomaly. The latter is better appreciated in the limit of  $\epsilon = 0$  (EP condition). For  $\epsilon \ll \omega_0$ , we can further expand up to leading order in  $\epsilon$  the denominator and get

$$\mathcal{W}_1 \approx -\frac{8\hbar\gamma_1\gamma_2}{|\omega - \omega_{EP}|^8} \left(\frac{\Delta\gamma}{2}\right)^2 [2\gamma_0(\omega - \omega_0) + \epsilon\Delta\gamma \left(1 - \frac{16(\omega - \omega_0)^2\gamma_0^2}{|\omega - \omega_{EP}|^4}\right)], \quad (13)$$

where the term associated with the perturbation  $\epsilon$  is an even function in  $(\omega - \omega_0)$ . We conclude, therefore, that the work density  $\mathcal{W}_\alpha$  loses the parity as soon as  $\epsilon$  is turned on, see also Fig. 2b. Below we will be discussing the consequences of such effect in the power extraction of the autonomous motor.

## VI. WORK IN THE PRESENCE OF EP

We are now ready to exploit the properties of  $\mathcal{W}_\alpha$  for the design of autonomous motors with optimal performance. To this end, we remind that the extracted work  $W$  is essentially the frequency integral of  $\mathcal{W}_\alpha$ , weighted with the function  $\tilde{\Theta}_\alpha(\omega)$ , see Eq. (5).

Let us first discuss the family of perturbations that preserve the (pseudo)- $\mathcal{PT}$ -symmetry of the unmodulated effective Hamiltonian. In this case, the antisymmetric form of the work density  $\mathcal{W}_\alpha$  with respect to the  $\omega_0$ -axis, results in a near-zero total work, see Fig. 2c. The slight deviation from zero (towards positive  $W > 0$ ) is due to the fact that Eq. (5) involves a product of  $\mathcal{W}_\alpha$  with  $\tilde{\Theta}(\omega)$  which slightly de-symmetrizes the integrand towards smaller frequencies (see continuous blue line). We can revert the situation by introducing a spectral filtering function  $\Phi(\omega)$  which enhances the unbalance contribution of positive and negative work densities in the integral of Eq. (5). The resulting extracted work, for the example case of a filter function  $\Phi(\omega) = H(\omega - \omega_0)$ , is

reported in Fig. 2c with a black dashed line ( $H(x)$  is the Heaviside function). Our results indicate that such a spectral filtering approach can lead to an increase in  $W$  which is higher by two orders of magnitude with respect to the unfiltered case. The same data indicate that the maximum work occurs in the vicinity of the EP where  $\mathcal{W}_\alpha$  acquires its maximum value (violet vertical line) and where the de-symmetrization strategy via spectral filtering is more impactful.

An alternative way to induce an asymmetric integrand in Eq. (5) is by perturbing the system away from the EP via a perturbation that will explicitly violate the (pseudo)- $\mathcal{PT}$  symmetry of the unmodulated effective Hamiltonian. In the previous section, we have identified one such perturbation being the frequency detuning  $\epsilon$  between the two resonators. In this case, the work density itself becomes asymmetric (see Fig. 2b), leading to a frequency integral Eq. (5) which is different from zero. In fact, the maximum  $W$  occurring in the proximity of  $\kappa_{EP}$ , is again two orders of magnitude enhanced in comparison to the  $\epsilon = 0$ -case, see the blue dashed line in Fig. 2c.

The enhancement of the extracted work  $W$  via engineered perturbations that violate the (pseudo)- $\mathcal{PT}$ -symmetry of the motor is better appreciated in Fig. 2d. Here, we report the extracted work  $W$  (for fixed  $\kappa = \kappa_{EP}$ ) for both spectrally unfiltered/filtered noise versus the perturbation  $\epsilon$ . For the unfiltered case (solid red line), we find that in the vicinity of the EP the total work is proportional to  $\epsilon$ , a relation that it is a direct consequence of the expansion Eq. (13) for the work density. Specifically, assuming for simplicity that  $\Theta_1(\omega) \approx \Theta_1(\omega_0)$ , the integration over  $\omega$  leads to the conclusion that  $W \approx A\Theta_1(\omega_0) \int d\omega/(2\pi)\mathcal{W}_1 \propto \epsilon$ . The same argument applies also in the case of spectral filtering with  $\Phi(\omega) = H(\omega - \omega_0)$  (see dashed red line). In both cases, the extreme work  $W_{\text{max}}$  occurs at perturbation strengths  $\epsilon_{\text{max}}$  in the vicinity of the EP, where the linear approximation Eq. (13) breaks down. An additional conclusion that we extract from the above analysis is that the spectral filtering method (combined with perturbations that violate the (pseudo)- $\mathcal{PT}$ -symmetry lead to a slightly (two-fold) increase of the extracted work as compared to the unfiltered case (see solid red line).

A panorama of the extracted work  $W$  versus  $\epsilon$  and  $\kappa$  is shown in Fig. 2e. Here we report only the unfiltered case i.e.  $\Phi(\omega) = 1$ . The data demonstrate nicely that the extreme value of the extracted work occurs in the vicinity of  $(\epsilon, \kappa) = (0, \kappa_{EP})$  where the EP is located. The case of spectral filtering with a function  $\Phi(\omega)$  (e.g.  $\Phi(\omega) = H(\omega - \omega_0)$ ) shows the same qualitative features (with the only difference that  $W$  is flat in the negative  $\epsilon$  semi-plane due to the specific filter function) and therefore is not reported here.

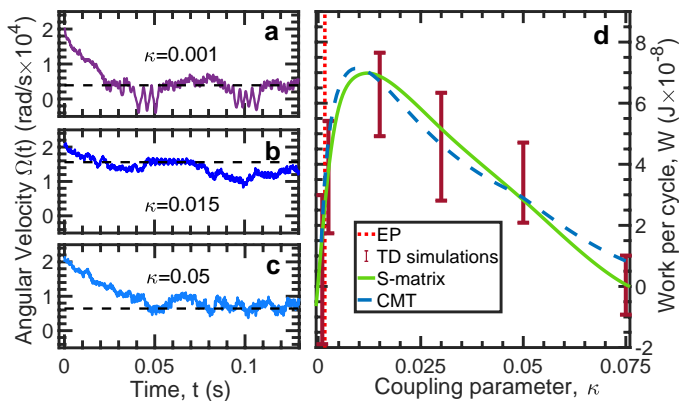


FIG. 3. (a-c) The dynamics of the angular velocity  $\Omega(t)$  for some representative values of the coupling coefficient  $\kappa$  whose terminal velocity determines the work delivered by the photonic circuit. (d) Work performed by the two-resonator circuit setup versus the coupling parameter  $\kappa$ . The numerical evaluation for the work (dots with error bars) is based on the value of the terminal angular velocity, see Eq. (14). The TD simulations match nicely the theoretical predictions for the work (green line) given by Eq. 5. The blue dashed line reports the work predicted by the CMT modeling, see Eqs. (3,8).<sup>48</sup> The vertical red dotted line indicates the position of the EP.

## VII. TIME DOMAIN SIMULATIONS AND IMPLEMENTATION USING ELECTROMECHANICAL SYSTEMS

We validate the above proposal by performing time-domain (TD) simulations using COMSOL software<sup>41</sup> with a realistic electromechanical system, see Fig. 1b. The setup consists of a pair of capacitively coupled resonators with impedance  $Z_0 = 70$  Ohm tuned at different frequencies,  $\omega_{1,2} = \omega_0 \pm \epsilon$ , which enforces violation of the (pseudo-)PT-symmetry of the unmodulated system. In our simulations, we have considered that  $\omega_0 = 2\pi f_0$ , with  $f_0 = 1$  MHz, and  $\epsilon = 0.0488 \cdot \omega_0$ . The capacitors  $C_{1,2}$  are considered as a pair of conductive plates separated by a median air gap  $d_0 = \frac{e_0 \cdot A}{C_0}$ , where  $e$  is the vacuum permittivity and  $C_0 = \frac{1}{Z_0 \cdot \omega_0}$  is a median capacitance. The upper plates of the capacitors are assumed to be attached to a wheel (the MDF) of radius  $r = d_0/10$  in a way that during the wheel rotation with angular velocity  $\Omega$  the plates will undergo a motion described by the displacements  $d_{1,2} = d_0 + r \cdot \cos(\phi_{1,2})$  with  $\phi_1 = \Omega t$  and  $\phi_2 = \phi_1 + \pi/2$ . The wheel is assumed to have mass  $m = 1$  g, moment of inertia  $I = 0.5 \cdot m r^2 = 7.58 \cdot 10^{-15}$  kg  $\cdot$  m<sup>2</sup>, and experiences friction with the ambient medium with friction coefficient  $\Gamma = 2.5 \cdot 10^{-13}$  N  $\cdot$  m  $\cdot$  s/rad. The coupling capacitance between the two LC resonators is  $C_c = 2\kappa \cdot C_0$ , where the coupling coefficient  $\kappa$  is a tunable parameter of the simulations. The left/right resonators are coupled to a hot/cold baths via capacitors  $C_{e1} = 0.1 \cdot C_0$ , and  $C_{e2} = 0.03 \cdot C_0$  respectively, which yields the following value for the critical coupling  $\kappa_{EP} = 0.001625$  (red dot-

ted line on Fig. 3d).

To enhance further the extracted work from the MDF we have introduced, in addition to the detuning  $\epsilon$ , spectral filtering of the thermal baths. Specifically, the hot bath is producing a noise signal consisting of 200 spectrally uniformly distributed harmonics  $V(t) = V_0 \cdot \sum_{i=1}^{200} \sin(\tilde{\omega}_i \cdot t + \varphi_i)$ , where  $V_0 = 1$  V is the amplitude of the noise,  $\tilde{\omega}_i$  is a frequency of each noise harmonic, and  $\varphi_i$  is a random phase shift. The lower frequency of the noise considered in the simulations is  $\tilde{\omega}_1 = 2\pi \cdot 0.85$  MHz with an upper limit of  $\tilde{\omega}_{200} = 2\pi \cdot 1.1$  MHz.

In the simulations the wheel is given an initial angular velocity  $\Omega_0 = 2.5 \cdot 10^4$  rad/s. Its angular velocity is monitored as a function of time until it saturates at a certain value  $\Omega_s$ . From here, we evaluate the work per cycle via the relation

$$W_{TD} = \int_0^{2\pi} \tau(x) dx = 2\pi \cdot \Gamma \cdot \Omega_s, \quad (14)$$

where  $\tau$  is the torque produced by the capacitor plates on the wheel and  $x$  is the angular displacement. The subindex TD indicates that the evaluated work is extracted from our time-domain simulations.

In Figs. 3a-c we show the transient dynamics of the angular velocity  $\Omega(t)$  for three typical coupling constants  $\kappa$ . Notice that in some cases (e.g Fig. 3a) the angular velocity  $\Omega(t)$  acquires negative values indicating that the wheel rotates opposite to the direction of the closed path  $\mathcal{C}$ . We find that in the long time limit the MDF reaches a terminal angular velocity  $\Omega(t \rightarrow \infty) \equiv \Omega_s^{TD}$  which can be used in Eq. (14) for the numerical evaluation of  $W_{TD}$ . In each of the subfigures 3a-c, we are also indicating (see dashed black line), the theoretical values of the saturation velocity  $\Omega_s$ . The latter has been extracted via Eq. (14), where the work  $W$  on the left-hand-side has been calculated using Eq. (5). For the theoretical evaluation of  $W$ , we have extracted the elements of the instantaneous S-matrix of the circuit using a frequency domain analysis of COMSOL<sup>41</sup>.

In Fig. 3d we report a summary of the extracted  $W_{TD}$  versus the coupling constants  $\kappa$ . The error bars reflect the fluctuations in the numerical evaluation of  $\Omega_s^{TD}$  and are extracted from the temporal analysis of  $\Omega(t)$  as  $\Omega_{min/max}^{TD} = \min/\max(\Omega(t \in [t_1, t_{max}]))$ , where  $t_1$  is the time during which  $\Omega(t)$  reaches the theoretical value of  $\Omega_s$  for the first time for a given value of  $\kappa$ ;  $t_{max} = 0.13$  s - is a maximum time used in a TD analysis. At the same figure, we are also plotting the theoretical predictions for the work  $W$  (green line) that have been derived using Eq. (5) with instantaneous scattering matrix elements given by the COMSOL frequency analysis of the electromechanical system. Finally, at the same figure, we are presenting the predictions of the CMT modeling of Eqs. (3,8). In the latter case, the various parameters (coupling, resonance frequencies, linewidths, etc.) of the CMT model have been extracted from the transmission spectrum of the electronic circuit (see methods). The

nice agreement between CMT and TD simulations confirm the validity of our CMT modeling and establishes the influence of the EP protocols in extracting maximum work from thermal autonomous motors.

### VIII. EFFICIENCY

The temperature gradient between the two thermal reservoirs induces a thermal current that goes through the motor. Part of the associated input power is dissipated due to friction, resulting in a reduction in the amount of *usable output power*<sup>35</sup>. The latter can be used e.g. for lifting a weight or charging a capacitor. The usable output power is

$$P_{\text{out}} = \frac{\Omega_s}{2\pi} W - \frac{\Omega_s}{2\pi} \Gamma \int_0^{\frac{2\pi}{\Omega_s}} \dot{x}^2 dt \approx \frac{\Omega_s}{2\pi} W - \Gamma \Omega_s^2, \quad (15)$$

where we have assumed that the MDF has large inertia, forcing the rotor to move with terminal velocity  $\dot{x} \approx \Omega_s$ . The optimal terminal angular velocity that maximizes the usable work is dictated by the parameters of the setup, and can be found from Eq. (15) to be  $\Omega_s^* = W/(4\pi\Gamma)$  leading to  $P_{\text{out}}^* = \left(\frac{W}{4\pi}\right)^2 \frac{1}{\Gamma}$ , which is half of the total “frictionless” power  $\left(\frac{W}{4\pi}\right)^2 \frac{2}{\Gamma}$ . For circuit parameters such that  $\Omega_s \gg \Omega_s^*$ , the motor dissipates most of the incident energy while in the other limiting case where  $\Omega_s \ll \Omega_s^*$  the friction can be neglected but the device does not generate much power. In both limits, the usable output power is nearly zero.

It is, therefore, useful to quantify the performance of an autonomous motor by introducing its efficiency  $\eta$ . The latter is defined as the ratio of the net usable average output power  $P_{\text{out}}$  that is extracted from the motor during one period of the cycle  $2\pi/\Omega_s^*$  when it operates under optimal conditions (i.e.  $\Omega_s = \Omega_s^*$ ), to the total input power  $P_{\text{in}}$  delivered to the photonic circuit. Specifically:

$$\eta^* \equiv \frac{P_{\text{out}}^*}{P_{\text{in}}}, \quad P_{\text{in}} \approx \bar{I}_b + \bar{I}_p \quad (16)$$

where for the evaluation of  $P_{\text{in}}$  we have also considered the fact that the slow variation of the photonic network’s parameters induces a pumping energy current  $\bar{I}_p$  in addition to the energy current  $\bar{I}_b$  due to the temperature bias<sup>42</sup>. Both currents above are measured at the hot reservoirs. Since typically  $\bar{I}_p \ll \bar{I}_b$  we can omit the pumped current from the denominator while we can substitute in Eq. (16) the maximum usable power as  $P_{\text{out}}^* \sim W^2/\Gamma$ . Therefore  $\eta^* \sim \left(\frac{W}{\bar{I}_b}\right) \frac{W}{\Gamma}$ , which suggests that the maximum  $\eta^* \leq \frac{\eta_C}{2}$  might be expected in the parameter domain where  $\bar{W}$  acquires its maximum values, see Figs. 2,3.

An efficient way to test the above expectations of the performance of our EP-influenced motor is by simultaneous evaluation of its efficiency Eq. (16) together with the corresponding power  $P_{\text{out}}^*$ . These quantities are plotted

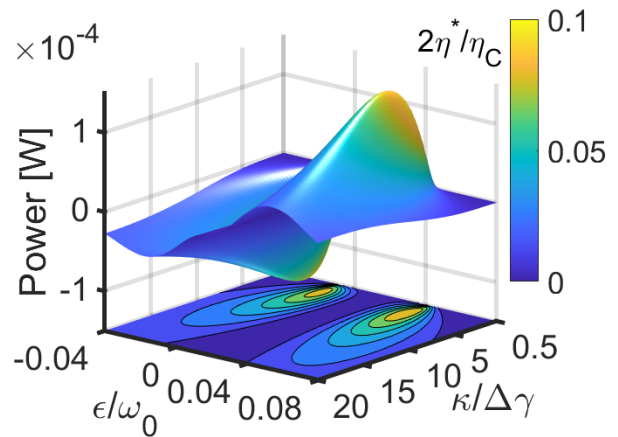


FIG. 4. Maximum power  $P_{\text{out}}^*$  (z-axis) and efficiency  $\eta^*$  normalized with respect to the maximum efficiency  $\eta_C/2$  (color-scale) at optimal operational conditions corresponding to  $\Omega_s = \Omega_s^*$ . These quantities are plotted as a function of the perturbation parameters  $\kappa$  and  $\epsilon$  for a fixed temperature gradient. The former perturbation respects the pseudo- $\mathcal{PT}$ -symmetric nature of the unmodulated system while the latter violates this symmetry. In these extensive simulations, we have used the CMT modeling with parameters associated with the circuit setup (see the previous section).

in Fig. 4 as a function of the perturbation parameters  $\kappa, \epsilon$  associated with the coupling and the resonance detuning between the two LC resonators of the electromechanical system of the previous section. For these calculations, we have used the CMT modeling with parameters that reproduce the results of the direct TD simulations of COMSOL for the electromechanical motor<sup>48</sup> (see Fig. 3d). Furthermore, we have ensured that the angular frequency  $\Omega_s^*$  is small enough such that the Born-Oppenheimer approximation is valid. From Fig. 4 we see that both  $\eta^*$  and  $P_{\text{out}}^*$  acquire their maximum values at the vicinity of the EP –albeit at slightly different  $(\kappa, \epsilon)$ -parameter values. This is because of a natural trade-off between efficiency and extracted power which has triggered a number of recent studies to identify conditions where this trade-off is optimized<sup>13,18,37,44–47</sup>. Our proposal shed new light in this direction since it identifies as an optimal domain for the design of cycles  $\mathcal{C}$ , the parameter space in the proximity of an EP.

### IX. CONCLUSIONS

We have theoretically proposed and numerically demonstrated, a dramatic enhancement of the performance of thermal motors when they are operating in a parametric domain which is in the proximity of an EP degeneracy. The latter appears in the spectrum of the effective non-Hermitian Hamiltonian that describes the open circuit and it is achieved via a judicious (differential) coupling of the isolated circuit with the ambient

baths. In the proximity of the EP, the eigenvector basis collapse (eigenvector degeneracy), leading to an enhanced spectral work density  $\mathcal{W}(\omega)$ . In typical circumstances,  $\mathcal{W}(\omega)$  is anti-symmetric with respect to the position of  $\omega_{EP}$  leading to a near-zero total work  $W$ . When, however, the spectral work density  $\mathcal{W}(\omega)$  is de-symmetrized, the total extracted power and the motor efficiency can acquire their maximum values in the domain of the parameter space which is in the vicinity of the EP. We have shown that this de-symmetrization can occur either via an explicit  $\mathcal{PT}$ -symmetry violation of the unperturbed system or via a spontaneous symmetry where, however, one needs to supplement it with additional spectral filtering of the radiation of the bath.

Our results pave the way towards the development of a new generation of optimal thermal motors that utilize engineered non-Hermitian spectral degeneracies. The

proposed scheme can find applications for on-chip photonics (e.g. self-powered micro-robots or micro-pumps in microfluidics), and electromechanical systems for harvesting ambient noise for powering a variety of auxiliary systems. It will be interesting to extend our study of motor efficiency to cases where the closed path in the parameter space is in the proximity of an EP degeneracy of higher order. It is plausible that the higher-order divergence of the resolvent will lead to a further enhancement of the total work. Similar questions emerge in the case where there are more than one EPs in the proximity of the closed path in the parameter space. The possibility to extend these design schemes for the realization of optimal quantum motors<sup>30</sup> is also another promising direction. These, and other, questions will be addressed in a separate publication.

- 
- <sup>1</sup> B. S. L. Collins, J. C. M. Kistemaker, E. Otten, B. L. Feringa, *A chemically powered unidirectional rotary molecular motor based on a palladium redox cycle.*, Nat. Chem **8**, 860 (2016).
- <sup>2</sup> M. R. Wilson, J. Solá, A. Carlone, S. M. Goldup, N. Lebrasseur, D. A. Leigh, Nature (London) **401**, 152 (1999)
- <sup>3</sup> N. Koumura, R. W. Zijlstra, R. A. van Delden, N. Harada, and B. L. Feringa, *Light-driven monodirectional molecular rotor*, Nature (London) **401**, 152 (1999).
- <sup>4</sup> M. Klok, N. Boyle, M. T. Pryce, A. Meetsma, W. R. Browne, B. L. Feringa, *MHz unidirectional rotation of molecular rotary motors*, J. Am. Chem. Soc. **130**, 10484 (2008).
- <sup>5</sup> H. L. Tierney, C. J. Murphy, A. D. Jewell, A. E. Baber, E. V. Iski, H. Y. Khodaverdian, A. F. McGuire, N. Klebanov, and E. C. H. Sykes, *Experimental demonstration of a single-molecule electric motor*, Nat. Nanotechnol. **6**, 625 (2011).
- <sup>6</sup> T. Kudernac, N. Ruangsapapichat, M. Parschau, B. Maciá, N. Katsonis, S. R. Harutyunyan, K.-H. Ernst, and B. L. Feringa, *Electrically driven directional motion of a four-wheeled molecule on a metal surface*, Nature (London) **479**, 208 (2011).
- <sup>7</sup> D. Palima, J. Glückstad, *Gearing up for optical micro-robotics: micromanipulation and actuation of synthetic microstructures by optical forces*, Laser Photon. Rev. **7**, 478 (2013).
- <sup>8</sup> D. M. Carberry, S. H. Simpson, J. A. Grieve, Y. Wang, H. Schäfer, M. Steinhart, R. Bowman, G. M. Gibson, M. J. Padgett, S. Hanna, M. J. Miles, *Calibration of optically trapped nanotools*, Nanotechnology **21**, 175501 (2010).
- <sup>9</sup> S. Kheifets, A. Simha, K. Melin, T. Li, M. G. Raizen, *Observation of Brownian motion in liquids at short times: instantaneous velocity and memory loss*, Science **343**, 1493 (2014).
- <sup>10</sup> T. Wu, T. A. Nieminen, S. Mohanty, J. Miotke, R. L. Meyer, H. Rubinsztein-Dunlop, M. W. Berns, *A photon-driven micromotor can direct nerve fibre growth*, Nature Photon. **6**, 62 (2012).
- <sup>11</sup> S. Carnot, *Réflexions sur la puissance motrice du feu et sur les machines propres à développer cette puissance* (Bachelier, Paris, 1824).
- <sup>12</sup> H. B. Callen, *Thermodynamics and An Introduction to Thermostatistics* (John Wiley & Sons, New York, 1985), 2nd ed.
- <sup>13</sup> F. L. Curzon and B. Ahlborn, *Efficiency of a Carnot engine at maximum power output*, Am. J. Phys. **43**, 22 (1975).
- <sup>14</sup> I. I. Novikov, At. Energ. 3, 1269 (1957) [J. Nucl. Energy II **7**, 125128 (1958)].
- <sup>15</sup> M. Esposito, R. Kawai, K. Lindenberg, and C. Van den Broeck, Phys. Rev. Lett. **105**, 150603 (2010).
- <sup>16</sup> B. Gaveau, M. Moreau, and L. S. Schulman, Phys. Rev. Lett. **105**, 060601 (2010).
- <sup>17</sup> U. Seifert, Phys. Rev. Lett. **106**, 020601 (2011).
- <sup>18</sup> G. Benenti, K. Saito, G. Casati, *Thermodynamic Bounds on Efficiency for Systems with Broken Time-Reversal Symmetry*, Phys. Rev. Lett. **106**, 230602 (2011).
- <sup>19</sup> D. Gelbwaser-Klimovsky and G. Kurizki, *Work extraction from heat-powered quantized optomechanical setups*, Sci. Rep. **5**, 07809 (2015).
- <sup>20</sup> A. Ronzani, B. Karimi, J. Senior, Y.-C. Chang, J. Peltonen, C.D. Chen, and J. P. Pekola, *Tunable photonic heat transport in a quantum heat valve*, Nature Phys. **14**, 991 (2018).
- <sup>21</sup> K. Zhang, F. Bariani, and P. Meystre, *Quantum Optomechanical Heat Engine*. Phys. Rev. Lett. **112**, 150602 (2014).
- <sup>22</sup> M. Serra-Garcia, A. Foehr, M. Moleron, J. Lydon, C. Chong, C. Daraio, *Mechanical Autonomous Stochastic Heat Engine*, Phys. Rev. Lett. **117**, 010602 (2016).
- <sup>23</sup> S. Beeby, M. Tudor, N. White, *Energy harvesting vibration sources for microsystems applications*, Measurement Science & Technology **17**, R175 (2006).
- <sup>24</sup> S. R. Anton, H. A. Sodano, *A review of power harvesting using piezoelectric materials*, Smart Materials and Structure **16**, 1 (2007)
- <sup>25</sup> P. Mitcheson, E. Yeatman, G. Rao, et al., *Energy harvesting from human and machine motion for wireless electronic devices*, Proceedings of the IEEE **96**, 1457 (2008).
- <sup>26</sup> N. Priya, D. Inman, *Energy Harvesting Technologies*, NY:Springer (2009)
- <sup>27</sup> T. V. Galchev, J. McCullagh, R. L. Peterson, K. Najafi, *Harvesting traffic-induced vibrations for structural health monitoring of bridges*, Journal of Micromechanics and Mi-

- croengineering **21**, 104005 (2011).
- <sup>28</sup> M. Wischke, M. Masur, M. Kroener, P. Woias, *Vibration harvesting in traffic tunnels to power wireless sensor nodes*, *Smart Materials and Structures* **20**, 8 (2011)
- <sup>29</sup> H. Haus, *Electromagnetic Noise and Quantum Optical Measurements* (Springer-Verlag, Berlin, 2000).
- <sup>30</sup> R. A. Bustos-Marun and H. L. Calvo, *Thermodynamics and steady state of quantum motors and pumps far from equilibrium*, *Entropy* **21**, 824 (2019).
- <sup>31</sup> R. Bustos-Marun, G. Refael, F. von Oppen, *Adiabatic Quantum Motors*, *Phys. Rev. Lett.* **111**, 060802 (2013).
- <sup>32</sup> D. Dundas, E. J. McEniry, and T. N. Todorov, *Current-driven atomic waterwheels*, *Nat. Nanotech.* **4**, 99 (2009).
- <sup>33</sup> N. Bode, S. Kusminskiy, R. Egger, F. von Oppen, *Scattering Theory of Current-Induced Forces in Mesoscopic Systems*, *Phys. Rev. Lett.* **107**, 036804 (2011).
- <sup>34</sup> L. J. Fernández-Alcázar, H. M. Pastawski, R. A. Bustos-Marín, *Dynamics and decoherence in nonideal Thouless quantum motors*, *Phys. Rev. B* **95** 155410 (2017).
- <sup>35</sup> L. J. Fernández-Alcázar, R. A. Bustos-Marín, H. M. Pastawski, *Decoherence in current induced forces: Application to adiabatic quantum motors*, *Phys. Rev. B* **92** 075406 (2015).
- <sup>36</sup> L. J. Fernández-Alcázar, H. M. Pastawski, and R. A. Bustos-Marín, *Nonequilibrium current-induced forces caused by quantum localization: Anderson adiabatic quantum motors*, *Phys. Rev. B* **99**, 045403 (2019).
- <sup>37</sup> K. Brandner, K. Saito, *Thermodynamic Geometry of Microscopic Heat Engines*, *Phys. Rev. Lett.* **124**, 040602 (2020).
- <sup>38</sup> B. Bhandari, P. Terrén Alonso, F. Taddei, F. von Oppen, R. Fazio, and L. Arrachea, *Geometric properties of adiabatic quantum thermal machines*, *Phys. Rev. B* **102**, 155407 (2020).
- <sup>39</sup> A. Guo, G. J. Salamo, D. Duchesne, R. Morandotti, M. Volatier-Ravat, V. Aimez, G. A. Siviloglou, D. N. Christodoulides, *Observation of  $PT$ -Symmetry Breaking in Complex Optical Potentials*, *Phys. Rev. Lett.* **103**, 093902 (2009).
- <sup>40</sup> A. Pick, B. Zhen, O. D. Miller, C. W. Hsu, F. Hernandez, A. W. Rodriguez, M. Soljačić, S. G. Johnson, *General theory of spontaneous emission near exceptional points*, *Opt. Express* **25**, 12325 (2017).
- <sup>41</sup> COMSOL Multiphysics v. 5.5., COMSOL AB, Stockholm, Sweden, [www.COMSOL.com](http://www.COMSOL.com) (2020).
- <sup>42</sup> H Li, L. J. Fernández-Alcázar, F. Ellis, B. Shapiro, T. Kottos, *Adiabatic Thermal Radiation Pumps for Thermal Photonics*, *Phys. Rev. Lett.* **123**, 165901 (2019).
- <sup>43</sup> A. P. Seyranian and A. A. Mailybaev, *Multiparameter Stability Theory With Mechanical Applications* (World Scientific Publishing, 2003, vol. XIII).
- <sup>44</sup> K. Brandner, K. Saito, U. Seifert, *Strong Bounds on Onsager Coefficients and Efficiency for Three-Terminal Thermoelectric Transport in a Magnetic Field*, *Phys. Rev. Lett.* **110**, 070603 (2013).
- <sup>45</sup> R. S. Whitney, *Most Efficient Quantum Thermoelectric at Finite Power Output*, *Phys. Rev. Lett.* **112**, 130601 (2014).
- <sup>46</sup> N. Shiraishi, K. Saito, H. Tasaki, *Universal Trade-Off Relation between Power and Efficiency for Heat Engines*, *Phys. Rev. Lett.* **117**, 190601 (2016).
- <sup>47</sup> P. Abiuso, M. Peramau-Llobet, *Optimal Cycles for Low-Dissipation Heat Engines*, *Phys. Rev. Lett.* **124**, 110606 (2020).
- <sup>48</sup> The CMT Hamiltonian's parameters that best fit scattering spectrums of the circuit setup are  $\gamma_1 \approx 3.6 \times 10^{-3}$ ,  $\gamma_2 \approx 3.2 \times 10^{-4}$ ,  $\omega_1 \approx 1 - \kappa$ , and  $\omega_2 \approx 0.94 - \kappa$ , in units of  $\omega_0 = 2\pi \times 1MHz$ . For a detailed model of the CMT see<sup>49</sup>
- <sup>49</sup> L. J. Fernández-Alcázar, H. Li, T. Kottos, *Extreme Non-Reciprocal Near-Field Thermal Radiation via Floquet Photonics*, <https://arxiv.org/abs/2006.12200>

# Supplementary Material: “Thermal Motors with Enhanced Performance due to Engineered Exceptional Points”

## SI. Expressions for forces and work

In this section we derive the expressions for the forces and work in terms of the instantaneous scattering matrix of the associated photonic network. In particular, we arrive to Eq. (5) of the main text.

The starting point is the definition of the force, Eq. (2) of the main text, which, in turn, requires the knowledge of the field amplitude. The later is given by the Coupled-Mode Theory (CMT) in Eq. (3). Here, we assume that the dynamical time scales of the mechanical degree of freedoms (MDFs)  $\vec{x}$  are much slower than the photonic time-scales, i.e., we invoke the Born-Oppenheimer approximation. Under this approximation, we have the CMT in frequency domain (we use the convention  $f(t) = \int_0^\infty f(\omega)e^{-i\omega t}d\omega$  for the Fourier transform)

$$\begin{aligned}\Psi(\omega) &= iG^{\vec{x}}(\omega)D^T\theta^{(+)}(\omega); \quad G^{\vec{x}} = (\omega I_N - H_{\text{eff}})^{-1}; \\ \theta^{(-)}(\omega) &= S^{\vec{x}}(\omega)\theta^{(+)}(\omega); \quad S^{\vec{x}}(\omega) = -I_{N_\alpha} + iDG^{\vec{x}}(\omega)D^T,\end{aligned}\tag{S1}$$

where  $I_m$  is the  $m \times m$  identity matrix and we assume that  $D$  and independent of  $\omega$  and  $\vec{x}$ . Here, the field amplitude  $\Psi$  and the outgoing scattering field  $\theta^{(-)}$  are dictated by the “frozen” or “instantaneous” effective Hamiltonian  $H_{\text{eff}} = H_0(\vec{x}) - i\frac{D^TD}{2}$ , the Green function  $G^{\vec{x}}(\omega)$ , and the Scattering matrix  $S^{\vec{x}}(\omega)$ . In order to keep the notation simple, from now on we will drop the index “ $\vec{x}$ ” and the dependence on  $\vec{x}$  of  $G^{\vec{x}} \equiv G$  and  $S^{\vec{x}} \equiv S$  will remain implicit.

We get the generalized force by starting from Eq. (2) and using Eqs. (S1) and (4)

$$\begin{aligned}\vec{F}_{\text{av}} &= -\hbar \int_0^\infty \frac{d\omega}{2\pi} \sum_\alpha \tilde{\Theta}_\alpha(\omega) [DG^\dagger(\nabla_{\vec{x}}H_0)GD^T]_{\alpha,\alpha} \\ &= \int_0^\infty \frac{d\omega}{2\pi} \sum_\alpha \tilde{\Theta}_\alpha(\omega) \left( \frac{\hbar}{i} S^\dagger \nabla_{\vec{x}} S \right)_{\alpha,\alpha},\end{aligned}\tag{S2}$$

where  $\alpha$  labels both, the reservoir and the resonator coupled to it. To arrive to the second line we used that<sup>S1</sup>

$$S^\dagger \nabla_{\vec{x}} S = -iDG^\dagger \nabla_{\vec{x}} H_0 G D^T,\tag{S3}$$

which can be probed by using Eq. S1 and by noticing that  $(G)^{-1} - (G^\dagger)^{-1} = iD^TD$  and  $\nabla_{\vec{x}}G = G\nabla_{\vec{x}}H_0G$ .

These equations are adequate to predict the forces and hence, energy extraction capabilities, benefiting from different experimental situations. While the first equation requires the energy distribution inside the resonators of the photonic circuit via the Green’s function, the second equation utilizes the scattering coefficients of the circuit.

Finally, we calculate the energy extraction capability of our motor,  $W = \oint_C \vec{F}_{\text{av}} \cdot d\vec{x}$ , by integrating the force when the generalized coordinates  $\vec{x}$  move along a path  $C$ , resulting in Eq. (5) of the main text.

## SII. Work density in terms of the Green’s functions

In this section we derive the analytical expression for the work density, Eq. (7) in terms of the Green’s functions. For simplicity, from now on we will consider that only diagonal elements of the Hamiltonian change with  $\vec{x}$ , i.e.  $(\nabla_{\vec{x}}H_0)_{n,m} = (\nabla_{\vec{x}}H_0)_{n,n}\delta_{n,m}$ . Next, we consider a driving protocol such that in our photonic network only two resonators are driven, which we denote with indexes  $n = p, q$ ; and each one of the resonant frequencies of those resonators  $\omega_n = (H_0)_{n,n}$  depend on only one coordinate  $x_\nu$ , i.e.  $\frac{\partial\omega_n}{\partial x_\nu} = \frac{\partial\omega_n}{\partial x_n}\delta_{n,\nu}$ . By using Eq. S2, we calculate the work as  $W = \oint_C \vec{F}_{\text{av}} \cdot d\vec{x} = \iint_A (\nabla_{\vec{x}} \times \vec{F}_{\text{av}}) \cdot d\vec{A}$ , i.e.,

$$\begin{aligned}W &= -\hbar \int_0^\infty \frac{d\omega}{2\pi} \sum_\alpha 2\gamma_\alpha \tilde{\Theta}_\alpha(\omega) \oint_C \left( |G_{p,\alpha}|^2 \frac{\partial\omega_p}{\partial x_p} dx_p + |G_{q,\alpha}|^2 \frac{\partial\omega_q}{\partial x_q} dx_q \right), \\ &= -\hbar \int_0^\infty \frac{d\omega}{2\pi} \sum_\alpha 2\gamma_\alpha \tilde{\Theta}_\alpha(\omega) \iint_A \left( \frac{\partial|G_{q,\alpha}|^2}{\partial x_p} \frac{\partial\omega_q}{\partial x_q} - \frac{\partial|G_{p,\alpha}|^2}{\partial x_q} \frac{\partial\omega_p}{\partial x_p} \right) dx_p dx_q,\end{aligned}\tag{S4}$$

where, to arrive to the second equality, we have used Green’s theorem. It is useful to turn Eq. S4 into a more compact expression by using the geometric integral  $P_\alpha$ , defined in Eq. (5). Finally, the work density per unit area

$$\mathcal{W}_\alpha = \lim_{A \rightarrow 0} \frac{P_\alpha}{A} = 4\gamma_\alpha \hbar \text{Re} (G_{p\alpha}^* G_{pq} G_{q\alpha} - G_{q\alpha}^* G_{qp} G_{p\alpha}),\tag{S5}$$

where, we have used  $\frac{\partial|G_{nm}|^2}{\partial x_j} = 2\text{Re} (G_{nm}^* G_{nj} \frac{\partial\omega_j}{\partial x_j} G_{jm})$ , and since  $A = \iint_A \frac{\partial\omega_p}{\partial x_p} \frac{\partial\omega_q}{\partial x_q} dx_p dx_q \rightarrow 0$ , the Green’s functions are evaluated at the center of the loop  $\{x_p, x_q\}$ .

### SIII. Green's function near the EP

When the path  $C$  is performed in the vicinity of an EP, the interplay of the coalescing resonances can dramatically affect the response of the system under small perturbations. This abrupt behavior can be related to the Green's function, which in the vicinity of a (second order) EP, presents a sharp Lorentzian-squared resonance, evidenced through the modal expansion around the EP<sup>S2</sup>

$$G(\omega) = \sum_n \frac{1}{\omega - \omega_n} \frac{\tilde{u}_n \cdot \tilde{v}_n^T}{\tilde{v}_n^T \cdot \tilde{u}_n} \approx \frac{A}{\omega - \omega_{EP}} + \frac{B}{(\omega - \omega_{EP})^2}. \quad (\text{S6})$$

To arrive to the right hand side, we assume  $\omega \approx \omega_{EP}$  and then we can restrict the summation to  $n$  indexes whose eigenfrequencies  $\omega_n$ , and the corresponding right (left) eigenvectors  $\tilde{u}_n$  ( $\tilde{v}_n$ ) of  $H_{\text{eff}}$ , are associated to the EP. To simplify the notation, we denote them by  $\omega_{\pm}$  and  $\tilde{u}_{\pm}$  ( $\tilde{v}_{\pm}$ ). Next, we use an expansion in a Newton-Puiseux series invoking fractional-powers of a perturbation parameter  $p \ll 1$ <sup>S3</sup>

$$\begin{aligned} \omega_{\pm} &= \omega_{EP} \pm p^{1/2} \lambda_1 + p \lambda_2 \pm p^{3/2} \lambda_3 + \dots, \\ \tilde{u}_{\pm} &= u_0 \pm p^{1/2} \lambda_1 u_1 + p w_2 \pm p^{3/2} w_3 + \dots, \end{aligned} \quad (\text{S7})$$

where a similar equation holds for  $\tilde{v}_{\pm}$  and the Hamiltonian  $H_{\text{eff}} = H_{\text{eff}}^T \approx H_0 + p H_1 + \dots$ . The EP occurs at  $p = 0$ , and there, the defective right (left) eigenvector  $u_0$  ( $v_0$ ) of  $H_0$  and the associated Jordan vector  $u_1$  ( $v_1$ ) satisfy the Jordan chain relations

$$\begin{aligned} H_0 u_0 &= \omega_{EP} u_0 ; H_0 u_1 = \omega_{EP} u_1 + u_0 \\ v_0^T H_0 &= \omega_{EP} v_0^T ; v_1^T H_0 = \omega_{EP} v_1^T + v_0^T, \end{aligned} \quad (\text{S8})$$

with the normalization conditions  $v_0^T u_1 = 1$  and  $v_1^T u_1 = 0$  and the properties  $v_0^T u_0 = 0$  and  $v_1^T u_0 = v_0^T u_1 = 1$ . It follows that  $\lambda_1 = \pm \sqrt{v_0^T H_1 u_0}$ , which determines the leading order of the expansions in Eqs. S7. By keeping these expansions up to leading order, we arrive to the right hand side of Eq. S6, where  $A = u_1 v_0^T + u_0 v_1^T$  and  $B = u_0 v_0^T$ .

- [S1] N. Bode, S. Kusminskiy, R. Egger, F. von Oppen, *Scattering Theory of Current-Induced Forces in Mesoscopic Systems*, Phys. Rev. Lett. **107**, 036804 (2011).
- [S2] A. Pick, B. Zhen, O. D. Miller, C. W. Hsu, F. Hernandez, A. W. Rodriguez, M. Soljačić, S. G. Johnson, *General theory of spontaneous emission near exceptional points*, Opt. Express **25**, 12325 (2017).
- [S3] A. P. Seyranian and A. A. Mailybaev, *Multiparameter Stability Theory With Mechanical Applications* (World Scientific Publishing, 2003, vol. XIII).